



**HAL**  
open science

## Atomic-scale understanding of high thermal stability of the Mo/CoFeB/MgO spin injector for spin-injection in remanence

Bingshan Tao, Philippe Barate, Xavier Devaux, Pierre Renucci, Julien Frougier, Abdelhak Djeflal, Shiheng Liang, Bo Xu, Michel Hehn, Henri Jaffrès, et al.

► **To cite this version:**

Bingshan Tao, Philippe Barate, Xavier Devaux, Pierre Renucci, Julien Frougier, et al.. Atomic-scale understanding of high thermal stability of the Mo/CoFeB/MgO spin injector for spin-injection in remanence. *Nanoscale*, 2018, 10 (21), pp.10213-10220. 10.1039/c8nr02250j . hal-02011611

**HAL Id: hal-02011611**

**<https://hal.univ-lorraine.fr/hal-02011611>**

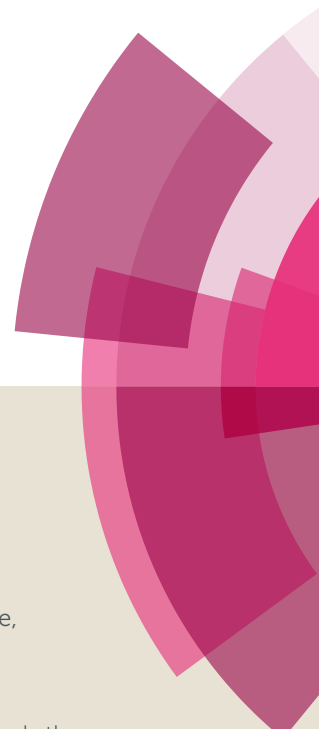
Submitted on 14 Mar 2019

**HAL** is a multi-disciplinary open access archive for the deposit and dissemination of scientific research documents, whether they are published or not. The documents may come from teaching and research institutions in France or abroad, or from public or private research centers.

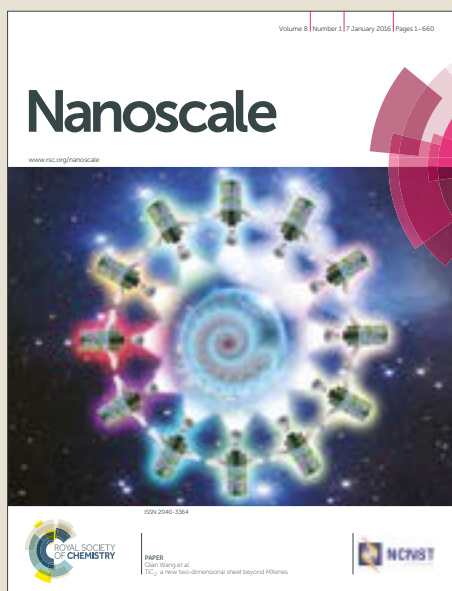
L'archive ouverte pluridisciplinaire **HAL**, est destinée au dépôt et à la diffusion de documents scientifiques de niveau recherche, publiés ou non, émanant des établissements d'enseignement et de recherche français ou étrangers, des laboratoires publics ou privés.

# Nanoscale

Accepted Manuscript



This article can be cited before page numbers have been issued, to do this please use: B. Tao, P. Barate, X. Devaux, P. Renucci, J. Frougier, A. Djeflal, S. Liang, B. Xu, M. Hehn, H. Jaffres, J. George, X. Marie, S. Mangin, X. Han, Z. Wang and Y. LU, *Nanoscale*, 2018, DOI: 10.1039/C8NR02250J.



This is an Accepted Manuscript, which has been through the Royal Society of Chemistry peer review process and has been accepted for publication.

Accepted Manuscripts are published online shortly after acceptance, before technical editing, formatting and proof reading. Using this free service, authors can make their results available to the community, in citable form, before we publish the edited article. We will replace this Accepted Manuscript with the edited and formatted Advance Article as soon as it is available.

You can find more information about Accepted Manuscripts in the [author guidelines](#).

Please note that technical editing may introduce minor changes to the text and/or graphics, which may alter content. The journal's standard [Terms & Conditions](#) and the ethical guidelines, outlined in our [author and reviewer resource centre](#), still apply. In no event shall the Royal Society of Chemistry be held responsible for any errors or omissions in this Accepted Manuscript or any consequences arising from the use of any information it contains.



## Nanoscale

## ARTICLE

## Atomic-Scale Understanding of High Thermal Stability of Mo/CoFeB/MgO Spin Injector for Spin-Injection in Remanence

Bingshan Tao<sup>a,e,f</sup>, Philippe Barate<sup>b</sup>, Xavier Devaux<sup>a</sup>, Pierre Renucci<sup>b</sup>, Julien Frougier<sup>c</sup>, Abdelhak Djeflal<sup>a</sup>, Shiheng Liang<sup>a</sup>, Bo Xu<sup>d</sup>, Michel Hehn<sup>a</sup>, Henri Jaffrès<sup>c</sup>, Jean-Marie George<sup>c</sup>, Xavier Marie<sup>b</sup>, Stéphane Mangin<sup>a</sup>, Xiufeng Han<sup>e\*</sup>, Zhanguo Wang<sup>d</sup> and Yuan Lu<sup>a\*</sup>

Received 00th January 20xx,  
Accepted 00th January 20xx

DOI: 10.1039/x0xx00000x

www.rsc.org/

Remanent spin injection in spin light emitting diode (spin-LED) at zero magnetic field is a prerequisite for future application of spin optoelectronics. Here, we demonstrate the remanent spin injection into GaAs based LED with thermally stable Mo/CoFeB/MgO spin injector. A systematic study of magnetic properties, polarization-resolved electroluminescence (EL) and atomic-scale interfacial structures has been performed in comparison with the Ta/CoFeB/MgO spin injector. The perpendicular magnetic anisotropy (PMA) of Mo/CoFeB/MgO injector shows much advanced thermal stability than that of Ta/CoFeB/MgO injector and robust PMA can be maintained up to 400°C annealing. The remanent circular polarization ( $P_C$ ) of EL from the Mo capped spin-LED reaches a maximum value of 10% after 300°C annealing, and even persists in 4% after 400°C annealing. On the contrary, the Ta capped spin-LED almost completely loses the remanent  $P_C$  under 400°C annealing. The combined advanced electron microscopy and spectroscopy studies reveals that a large amount of Ta diffuses into the MgO tunneling barrier through CoFeB layer after 400°C annealing. However, the diffusion of Mo into CoFeB is limited and never reaches the MgO barrier. These findings afford a comprehensive perspective to use the high thermally stable Mo/CoFeB/MgO spin injector for an efficient electrical spin injection in remanence.

### 1. Introduction

Spin light emitting diode (spin-LED)<sup>1</sup> technology is an important class of semiconductor spintronic devices, which encodes the electron spin information into circularly polarized light and shows strong potential applications in advanced semiconductor

technologies such as optical transport of information,<sup>2</sup> quantum cryptography<sup>3</sup> and three-dimensional display.<sup>4</sup> Spin-LED was firstly demonstrated in GaAs based LEDs with paramagnetic<sup>5</sup> and ferromagnetic<sup>6</sup> semiconductor injectors at low temperature. Subsequently, many kinds of spin-injector employing common ferromagnetic (FM) 3d-transition metals, such as Fe,<sup>7-13</sup> Co,<sup>14,15</sup> CoFe,<sup>16-18</sup> and CoFeB,<sup>19,20</sup> were developed to obtain circularly polarized light at room temperature. However, the conductance mismatch between FM and semiconductors generally limits the spin injection efficiency severely.<sup>21</sup> It has been shown that this issue can be solved by inserting a tunnel barrier layer between the FM injector and the semiconductor,<sup>22,23</sup> such as Schottky barrier,<sup>7-12,14</sup> AlO<sub>x</sub><sup>10,13,15-17</sup> and MgO<sup>18-20</sup>. A high circular polarization  $P_C$  of about 30% at room temperature has been reported using CoFe/MgO injectors.<sup>18</sup> According to the optical selection rules,<sup>24,25</sup> the magnetization of the spin injector has to be maintained perpendicular to the quantum well (QW) LED surface in order to emit a circularly polarized light from the surface emission geometry. This usually requires a strong external magnetic field up to several Tesla to keep the perpendicular magnetization. For practical application, it is important to realize remanent spin injection at zero or small magnetic field, which demands the development of spin

<sup>a</sup> Institut Jean Lamour, UMR 7198, CNRS-Université de Lorraine, Campus ARTEM, 2 Allée André Guinier, BP 50840, 54011 Nancy, France

Email: yuan.lu@univ-lorraine.fr

<sup>b</sup> Université de Toulouse, INSA-CNRS-UPS, LPCNO, 135 avenue de Rangueil, 31077 Toulouse, France

<sup>c</sup> Unité Mixte de Physique, CNRS, Thales, Univ. Paris-Sud, Université Paris-Saclay, 1 Avenue A. Fresnel, 91767 Palaiseau, France

<sup>d</sup> Key Laboratory of Semiconductor Materials Science, Institute of Semiconductors, University of Chinese Academy of Sciences, Chinese Academy of Sciences, P. O. Box 912, Beijing 100083, China

<sup>e</sup> Beijing National Laboratory of Condensed Matter Physics, Institute of Physics, University of Chinese Academy of Sciences, Chinese Academy of Sciences, Beijing 100190, China

Email: xfhan@iphy.ac.cn

<sup>f</sup> Institute of Electrical Engineering, Chinese Academy of Sciences, Beijing 100190, China

\*Electronic Supplementary Information (ESI) available: See DOI: 10.1039/x0xx00000x

injectors with perpendicular magnetic anisotropy (PMA) to overcome the demagnetization field which tend to maintain the magnetization in plane. Results involving several kinds of spin injectors with PMA including Fe/Tb,<sup>26,27</sup> Co/Pt,<sup>28,29</sup> FePt<sup>30</sup> and  $\delta$ -MnGa<sup>31</sup> with either Schottky or MgO barrier have been reported. However, the remanent  $P_C$  is only limited at 3%~4% due to the low spin polarization at the FM/semiconductor interface.

In our previous work,<sup>32</sup> we have demonstrated large and robust remanent spin injection into GaAs based LED via Ta/CoFeB/MgO spin injectors with strong PMA thanks to the interfacial anisotropy at the FM/oxide interface.<sup>33</sup> Furthermore, a perpendicular magnetic tunnel junction (MTJ) type spin-injector has also been developed for future electrical control of spin-injection direction.<sup>34</sup> The key role of the Ta layer to absorb boron (B) and establishing the PMA property has been demonstrated.<sup>32-34</sup> However, the PMA of Ta/CoFeB/MgO system suffers from insufficient thermal stability at annealing temperature higher than 300°C,<sup>32,35,36</sup> which limits the achievement of even higher spin-injection efficiency and future integration into semiconductor industrial production. Some future applications also require the spin-injector to work in high temperature environments (such as in space). Although the information of the relationship between the PMA properties and nanoscale structures is of significance to enhance the performance of spin injector, as so far, no systematic structural and chemical analyses have been performed to explore the mechanism of annealing on the PMA properties of spin-injector in the spin-LED system at the atomic-scale level.

In experiments, several alternative capping layers have been explored to improve the thermal stability,<sup>37-40</sup> among which Mo showing good stability with thermal treatment up to 425°C.<sup>40</sup> In this work, we employ Mo as capping layer to develop perpendicular Mo/CoFeB/MgO spin injectors and study systematically its characteristics in comparison with Ta/CoFeB/MgO spin injector. The polarization-resolved electroluminescence (EL) spectra of the spin-LEDs with the two types of spin injectors annealed at different temperature were measured. High resolution scanning transmission electron microscopy (HR-STEM) combined with spatially resolved electron energy loss spectroscopy (EELS) was performed to characterize the interfacial structure and element distribution in both types of spin-injectors at atomic level. By linking the information of the structure and local chemical composition of the spin injectors to the measured magnetic and polarization-resolved EL properties, we develop a comprehensive way towards an efficient and optimized electrical spin injection in remanence.

## 2. Experimental methods

The structure of spin-LED consists of two parts: the semiconducting LED part and the metallic spin-injector part, as schematically shown in Figure 1a. The  $p$ - $i$ - $n$  LED with single quantum well was grown by molecular beam epitaxy (MBE) with the following structure:  $p$ -GaAs:Zn (001) substrate ( $p=2\times 10^{19}\text{cm}^{-3}$ ) /500 nm  $p$ -GaAs:Be ( $p=2\times 10^{19}\text{cm}^{-3}$ ) /200 nm  $p$ -GaAs:Be ( $p=2\times 10^{18}\text{cm}^{-3}$ ) /50 nm undoped GaAs/10 nm undoped  $\text{In}_{0.1}\text{Ga}_{0.9}\text{As}$ /50nm undoped GaAs/50 nm  $n$ -GaAs:Si ( $n=1\times 10^{16}\text{cm}^{-3}$ ). The LED surface was passivated with arsenic and then transferred

into another MBE-sputtering interconnected system through air to deposit the spin injector part. The arsenic was firstly desorbed by heating in MBE chamber monitored by reflective high energy electron diffraction (RHEED) until clear Kikuchi patterns appear to certificate a perfect crystalline GaAs surface. Then the sample was transferred to the sputtering chamber without breaking vacuum to grow the spin-injector multilayer with a structure of MgO(2.5 nm)/Co<sub>40</sub>Fe<sub>40</sub>B<sub>20</sub>(1.1 nm)/Ta(5 nm) or MgO(2.5 nm)/CoFeB(1.1 nm)/Mo(5 nm), as shown in Figure 1a, hereafter named as Ta injector and Mo injector, respectively. The effect of annealing at different temperature was investigated. The annealing processes were performed in rapid thermal annealing (RTA) system with a fixed duration time of 3 minutes at each temperature.

To measure the EL spectra, the spin-LED was patterned into circular mesas with 300 $\mu\text{m}$  diameters by UV lithography combined with etching technologies. The patterned spin-LED was placed into a Helmholtz split magnetic coil, providing a maximum magnetic field of 0.8T normal to the sample plane. The EL signal was detected in the Faraday geometry. The EL circular polarization ( $P_C$ ) was analyzed through a  $\lambda/4$  wave plate and a linear analyzer, which is defined as  $P_C = (I^{\sigma^+} - I^{\sigma^-}) / (I^{\sigma^+} + I^{\sigma^-})$ , where  $I^{\sigma^+}$  and  $I^{\sigma^-}$  are the intensity of the right and left circularly polarized components of the luminescence, respectively.

HR-STEM combined with spatially resolved EELS was performed by using a probe-corrected microscope JEOL ARM200F (cold FEG) equipped with a GATAN GIF quantum energy filter to reveal the structure and element distribution in the spin-injector before and after annealing. The microscope was operated at 200kV. High angle annular dark-field (HAADF), annular dark-field (ADF) and bright-field (BF) images were simultaneously recorded for structure study while only HAADF signal was recorded during EELS chemical analysis. Cross-sections for STEM observations were prepared by conventional mechanical polishing and Ar-ion milling.

## 3. Results and discussion

### 3.1 Magnetic Property Characterization of Spin-Injectors

A post-annealing treatment was essentially important to initialize the crystallization of CoFeB electrode and establish the perpendicular magnetic anisotropy.<sup>32-34</sup> The spin-LED film samples were cut into pieces and we carried out the annealing procedure in a rapid temperature annealing (RTA) system at different temperatures with a fixed duration of 3mins. The magnetic properties were characterized by superconducting quantum interference device (SQUID) with out-of-plane magnetic field ( $\mu_0H$ ) at room temperature (RT) and 10K. Figure 1b and 1c show the normalized  $M$ - $H$  curves of Ta and Mo injectors before and after annealed at different temperature ( $T_a$ ) from 250°C to 400°C, respectively. It can be seen that both Ta and Mo injectors show an in-plane anisotropy before annealing and the easy axis change to out-of-plane after annealing at 250°C. For Ta injectors, the PMA starts to degrade after annealing at 300°C and decreases rapidly with increasing annealing temperature, which is in agreement with our previous results.<sup>32</sup> However, for Mo injectors, there is only a slight change of the  $M$ - $H$  curves when  $T_a$  varies from 250°C to 400°C for both at RT and 10K, which indicates a much better thermal stability for Mo injector. In both cases, the PMA is enhanced at low

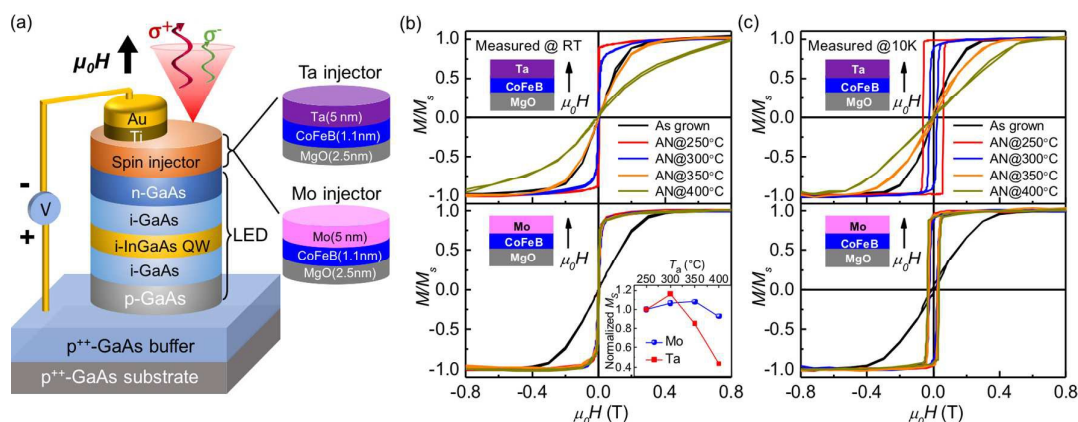


**Figure 1.** Magnetic characterization of spin-injectors. (a) Schematics of spin-LED structure with Ta or Mo capped spin-injector. (b)  $M$ - $H$  curves measured at RT for Ta and Mo spin-injectors before and after annealed at different temperatures. For short, “AN” represents for annealing. Inset: normalized  $M_s$  of Ta and Mo spin-injectors at RT as a function of annealing temperature. (c)  $M$ - $H$  curves measured at 10K for Ta and Mo spin-injectors before and after annealed at different temperatures.

temperature, as indicated from the enlarged coercivity at 10K. If we only compare the two injectors after an annealing procedure at 250°C, it is found that the PMA of Ta injector displays better properties than that of Mo injector, as indicated by the larger coercivity and remanent magnetization at 10K. However, the Mo injector shows much better PMA properties when annealed at higher temperature. This behaviour is also reflected by the tendency of the saturation magnetization ( $M_s$ ) vs.  $T_a$  measured at RT, as shown in the inset of under panel of Figure 1b. The  $M_s$  is normalized by the value at  $T_a=250^\circ\text{C}$ . It is found that the  $M_s$  of Ta injector firstly increases at  $T_a=300^\circ\text{C}$  and then decreases dramatically with increasing of  $T_a$ , while the Mo injector only exhibits a slight variation of  $M_s$  with different annealing temperatures. The increase of  $M_s$  is mainly due to the absorption of B from CoFeB layer to the capping layer to form the crystallized CoFe composition, while the decrease of  $M_s$  is attributed to the diffusion of capping layer elements (Ta or Mo) into the CoFeB layer process associated to the formation of some magnetic dead structures. We will show more evidences of that process with EELS characterizations below. In a first simple scenario, we can perceive that the better thermal stability of PMA for Mo injector could be attributed to the smaller diffusion of Mo into CoFeB layer at high annealing temperature.

### 3.2 Electroluminescence Characterization of Spin-LED

Figure 2a shows the typical EL spectra measured at 10K with  $\mu_0H=0$  for Mo spin-LED annealed at 300°C. The top (bottom) panel corresponds to the situation that the sample was firstly saturated with a positive (negative) magnetic field of 0.5T. A main EL peak at about 867 nm is observed, which corresponds to the heavy-hole exciton line. It is clear that there is an evident difference between the intensity of the right ( $\sigma^+$ ) and left ( $\sigma^-$ ) circularly polarized components at the main peak and a remanent circular polarization ( $P_c$ ) can be measured to be +9.5% in the top panel and -9.3% in the bottom panel. The large remanent  $P_c$  proves the high efficiency of spin injection from the Mo spin-injector. The sign change for  $P_c$  is directly linked to the reversal of the CoFeB magnetization when it is

magnetized in opposite direction after switching. Note that the contribution of magnetic circular dichroism (MCD) effect caused by the ferromagnetic CoFeB layer is estimated to be less than 1%.<sup>32</sup> Figure 2b displays the bias voltage ( $V_{\text{bias}}$ ) dependence of  $P_c$  at 0.5T for the Mo-based spin LED after annealing at 300°C. The bias dependence shows a gradual decreasing trend for  $P_c$  at high bias, which is mainly attributed to the smaller spin lifetime (due to the Dyakonov-Perel spin-relaxation mechanism<sup>18</sup>) for carriers injected into GaAs with a large kinetic energy at large bias.<sup>41</sup>

To check the thermal stability, we have measured the properties of the Mo spin-LED annealed at 400°C. Figure 2c displays the  $P_c$ - $H$  loop in comparison with the  $M$ - $H$  loop in a small field range. After

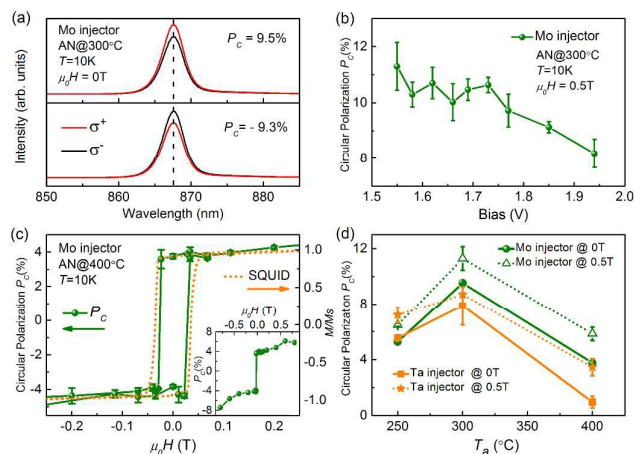


**Figure 2.** Polarization-resolved electroluminescence characterization. (a) EL spectra measured at 10K with  $\mu_0H=0$  for Mo spin-LED annealed at 300°C. The top (bottom) panel corresponds to the situation where the sample was firstly saturated with a positive (negative) magnetic field of 0.5T. (b) Bias dependence of  $P_c$  measured at 10K under 0.5T field for Mo spin-LED annealed at 300°C. (c)  $P_c$ - $H$  loop in comparison with  $M$ - $H$  loop in a small field range for Mo spin-LED annealed at 400°C. Inset:  $P_c$ - $H$  loop at large magnetic field range. (d)  $P_c$  as a function of annealing temperature

measured at zero and 0.5T magnetic field for Ta and Mo spin-injectors.

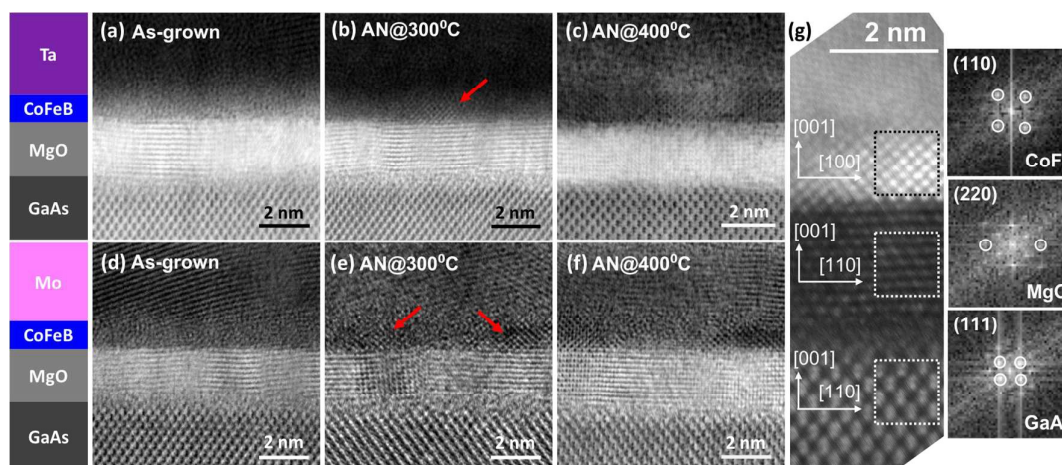


**Figure 3.** Structural characterization of spin-injectors. Bright field HR-STEM images of Ta injectors for: (a) as-grown state, (b) after annealing at 300°C and (c) 400°C. Bright field HR-STEM images of Mo injectors for: (d) as-grown state and (e) after annealing at 300°C and (f) 400°C. Zones where the CoFeB layer starts to crystallize from the CoFeB/MgO interface are indicated with red arrows in (b) and (e). (g) Dark field HR-STEM image for Mo injector after 400°C annealing in the zone where the CoFeB is well crystallized. A good epitaxial relationship GaAs[110](001)//MgO[110](001)//CoFe[100](001) can be found from the analysis of FFT diffraction patterns.

400°C annealing, the remanent  $P_C$  can still persist in 4%. The  $P_C$ - $H$  loop matches well with the  $M$ - $H$  loop, which again proves that the remanent  $P_C$  is directly linked to the remanent perpendicular magnetization of the Mo injector. The inset of Figure 2c shows the  $P_C$ - $H$  loop at large field range, where the  $P_C$  value gradually increases at high magnetic field. From our previous study,<sup>42</sup> it is known that the  $P_C$  measurement is very sensitive to the CoFeB/MgO interface while SQUID measurement relies on the whole CoFeB layer. The increase of  $P_C$  at high field could indicate that there still exists partially in-plane magnetization component (tilt) at the CoFeB/MgO interface.

In order to explore the effect of annealing and compare the performance between the Mo injector and the conventional Ta injector, we plot the  $P_C$  as a function of annealing temperature measured at zero and 0.5T magnetic field for the two kinds of injectors in Figure 2d. The  $P_C$  values were recorded at optimal bias for each annealing temperature. The circular polarization increases firstly from  $T_a=250^\circ\text{C}$  to  $T_a=300^\circ\text{C}$  and then decreases at  $T_a=400^\circ\text{C}$  for both injectors. The largest  $P_C$  value is obtained at  $T_a=300^\circ\text{C}$  for Ta injector despite of little degradation of the PMA. This is due to the better CoFeB/MgO interface after annealing at 300°C, resulting in higher spin injection efficiency. It is found that the  $P_C$  at 0.5T is always larger than that measured at zero field. Their difference is enlarged at  $T_a=400^\circ\text{C}$ , which means that the annealing will degrade the PMA and a part of magnetization returns in plane or becomes paramagnetic. At  $T_a=250^\circ\text{C}$ , both types of injectors have comparable  $P_C$ . However, the advantage of Mo injector is highlighted at high annealing temperature. Especially, at  $T_a=400^\circ\text{C}$  the Ta injector almost loses remanent  $P_C$  (<1%), while Mo injector can still remain 4% of  $P_C$ . This comparison undoubtedly validates the excellent thermal stability of Mo injector.

### 3.3 Structural Characterization of Spin-Injectors

In order to understand the mechanism related to the high thermal stability of Mo injector, we have performed HR-STEM and EELS for a detailed interfacial structural and chemical distribution study. Figure 3a-c and 3d-f show the bright field HR-STEM cross section images of Ta and Mo injectors before and after annealing at 300°C and 400°C, respectively. As shown in Figure 3a and 3d for both type of injectors before annealing, MgO layer has a good (001) textured structure, which is essential to act as a template for the crystallization of CoFeB layer with good orientation for PMA during annealing.<sup>43,44</sup> The ultrathin CoFeB layer appears continuous and amorphous and possesses very sharp interface with the MgO layer. The most important difference in structure between the two kinds of injectors is that the Ta capping layer is amorphous while the Mo capping layer is crystalline with a textured structure at the as-grown state. After annealing at 300°C, the CoFeB layer starts to crystallize from the CoFeB/MgO interface (indicated with red arrows in Figure 3b and 3e), where MgO serves as the template for the crystallization. After an annealing procedure at 400°C, the crystallization of CoFeB is better for Ta injector, which shows a complete crystallization in the whole CoFeB layer with a smooth interface with the Ta layer (Figure 3c). The crystallization state of the CoFeB layer is also improved for the Mo injector after 400°C annealing (Figure 3f) even though the CoFeB layer does not appear with the same crystalline quality as for the Ta capped injector. Zones close to the Mo capping layer are still amorphous. In the zone where the CoFeB is well crystallized with the Mo capping layer at  $T_a=400^\circ\text{C}$  (Figure 3g), a good epitaxial relationship can be found between GaAs, MgO and CoFeB layers. From the analysis of FFT diffraction patterns, an epitaxial relationship can be determined as GaAs [110] (001) // MgO [110] (001) // CoFe [100] (001), which is the same as that with Ta capping layer. Although Mo layer is also textured, it seems that a very thin amorphous layer still exists at the

Mo/CoFeB interface, which decouples the crystalline relationship between the Mo and the CoFeB layer.

### 3.4 Chemical Characterization of Spin-Injectors

STEM combined with EELS analysis is a very powerful tool to map the chemical information at the atomic level so that the inter-diffusion related to the annealing process can be understood in the

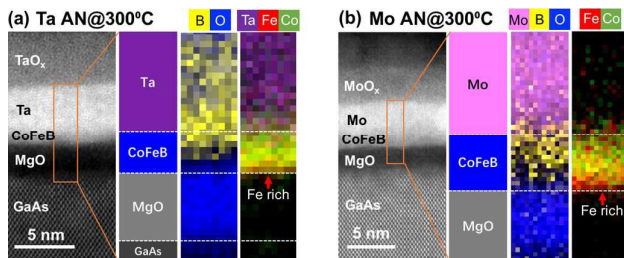


**Figure 4.** Chemical characterization of spin-injectors annealed at 300°C. Dark field HR-STEM images and corresponding EELS mappings for (a) Ta and (b) Mo injectors annealed at 300°C. The chemical elements are mapped from EELS spectrum images by extracting the signals of  $B_K(188\text{eV})$ ,  $Fe_{L3}(708\text{eV})$ ,  $Co_{L3}(779\text{eV})$ ,  $O_K(532\text{eV})$ ,  $Ta_{N5}(229\text{eV})$ ,  $Mo_{M5}(227\text{eV})$  edges. The corresponding colors of each element are labeled on the top of the images. Note that in the maps with Fe and Co elements, the color appears yellow when Fe and Co elements coexist. One or two monolayers with an enrichment of Fe at the CoFeB/MgO interface are indicated with red arrows.

nanostructure of spin injector. More detailed data on experimental EELS mapping and on the spectra analysis can be found in the Supporting Information. Figure 4 shows the dark field HR-STEM images and the corresponding element maps extracted from the EELS spectra for the Ta and Mo injectors annealed at 300°C. The elements shown in chemical maps and their corresponding colors are labeled on the top of the images. Due to the low solubility of B atoms in the CoFe host, the crystallization of CoFeB requires to eject out B atoms from CoFeB during annealing.<sup>45,46</sup> Indeed, as shown in Figure 4a for the Ta injector after 300°C annealing, the B (in yellow) diffuses out of CoFeB and appears homogeneously in the Ta layer. On the contrary, for the Mo injector, the B cannot efficiently penetrate into the Mo layer (in pink) and it still stays in the CoFeB layer with a tendency to accumulate at the Mo/CoFeB interface (Figure 4b), which delays or prevents the CoFeB crystallization in this area. The different behaviors of B can be explained by the different solubility of B in amorphous Ta and crystalline Mo layer. Therefore, the Ta injectors are revealed to be more efficient to absorb B favoring the crystallization of CoFeB layer, and this agrees well with what we observed of a better crystallization for Ta injector in HR-STEM images. In addition, an enrichment of Fe is observed at the CoFeB/MgO interface for both types of injectors. For the Mo injector, the composition ratio is estimated to be about Fe:Co=68:32 at the CoFeB/MgO interface and Fe:Co=45:55 in the CoFeB middle region. This could be due to the slight higher bond stability for Fe-O than Co-O, since the bond dissociation energy is 407.0 kJ/mol and 397.4 kJ/mol for Fe-O and Co-O bonds, respectively.<sup>47</sup>

At higher annealing temperature ( $T_a=400^\circ\text{C}$ ), the element diffusion becomes much enhanced. Figure 5 shows the EELS mapping and profile of different elements for Ta and Mo injectors annealed at 400°C. In the case of Ta injector, B concentration is too low to be detectable. As shown in Figure 5a, it is found that there is a significant Ta diffusion through the CoFeB into the MgO layer, up to the GaAs layer. The profile of the averaged integration of Ta peak is shown in Figure 5a to semi-quantitatively present the distribution of Ta in the spin injector. It is interesting to note that the concentration of Ta is higher in the MgO layer than in the CoFeB layer, which means that MgO can act as a sink to pump Ta. This could be due to an easy formation of  $Mg_xTa_yO_z$  oxide. However, no Ta can be found in GaAs layer. Compared to Ta injectors, B species are still detectable in Mo injectors, which mainly reside in the CoFeB layer and close to the Mo/CoFeB interface. More remarkably, the Mo spin injector displays few Mo diffusion at  $T_a=400^\circ\text{C}$ . As shown in Figure 5b, although some Mo atoms are detectable close to the Mo/CoFeB interface, Mo cannot fully penetrate into CoFeB layer to reach the CoFeB/MgO interface. Furthermore, no Mo can be detected in the MgO and GaAs layers. It is worth noting that the Fe-rich disappears in the Ta injector but still remains in the Mo injector after annealing at 400°C. The disappearance of Fe-rich character also can be attributed to the diffused Ta, which replace the Fe-O bonding by Ta-O bonding (bond dissociation energy: 810.4 kJ/mol). These results directly prove the high thermal stability of Mo injector, which is in very good agreement with the magnetic and circular polarization measurements.

### 3.5 Discussions

In order to obtain good performance for practical application without magnetic field, the key requirement for spin-injectors demands possessing both perpendicular magnetic anisotropy and also an efficient spin-polarization for spin-injection. Since the PMA property and quality is determined by the hybridization of O 2p and Fe(Co) 3d orbitals at the CoFeB/MgO interface,<sup>32,48</sup> the annealing process results in the expelling of B from CoFeB to promote the formation of Fe-O or Co-O bonds at the interface, producing the PMA and making CoFeB perpendicularly magnetized. When  $T_a < 300^\circ\text{C}$ , Ta injector is more efficiently to absorb B than Mo injector, which gives better PMA than Mo injector. However, after annealing at 400°C, a large amount of Ta diffuses towards CoFeB/MgO interface, which seriously degrades the PMA properties. On the contrary, the Mo diffusion is quite limited at high annealing temperature and few Mo can be detected at the CoFeB/MgO interface. Therefore, the PMA properties of Mo injector almost have not been affected after high temperature annealing.

In our previous study,<sup>42</sup> we have demonstrated that the control of the CoFeB/MgO interface is essential for an optimal and efficient spin injection into semiconductors. In fact, the spin-polarization at the CoFeB/MgO interface determines how much electron spin-polarization may be injected into the semiconductor part. After a 300°C annealing procedure, the CoFeB starts to crystallize at the CoFeB/MgO interface with the template of MgO layer in both types of injectors. Therefore, both injectors possess a high efficiency for spin-polarization injection, leading to comparable

circular polarization  $P_C$ . However, after a 400°C annealing procedure, the situation becomes quite different. Due to the large Ta diffusion into the CoFeB layer, the magnetic moment of CoFeB decreases by 60% because of the formation of some magnetic dead structures. These magnetic dead structures distributed in the whole CoFeB layer can effectively depolarize electron spin-polarization at the CoFeB/MgO interface. However, the change of magnetic moment for Mo injector is less than 10%. Together with the much less Mo diffusion found in EELS analysis, we can conclude that the

magnetic dead structures at the CoFeB/MgO interface for the Mo injector should be negligible, and the Mo injector can maintain high spin-polarization injection after high temperature annealing. In principle, we could get even higher  $P_C$  compared to  $T_a=300^\circ\text{C}$  since the annealing should improve the chemical structure at the CoFeB/MgO interface and get even higher spin-polarization, as demonstrated in Mo capped CoFeB/MgO/CoFeB MTJ systems.<sup>49</sup> However, in our case, the

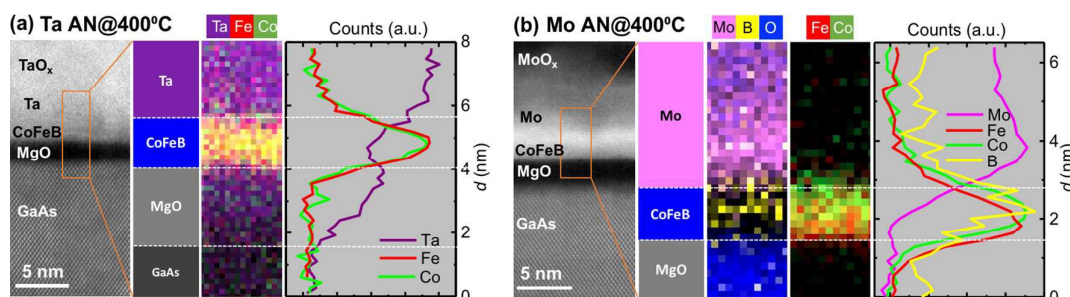


**Figure 5.** Chemical characterization of spin-injectors annealed at 400°C. Dark field HR-STEM images and corresponding EELS mappings and profiles for (a) Ta and (b) Mo injectors annealed at 400°C. The elements shown in chemical maps and their corresponding colors are labeled on the top of the images. The profiles are drawn by the integration of the element signal in the EELS mapping from an area of 1 pixel in height and 8 pixels in width, corresponding to the area of 0.2 nm in height and 1.6 nm in width.

decrease of  $P_C$  at  $T_a=400^\circ\text{C}$  for Mo injector could be related to the inter-diffusion in the semiconductor LED part (see Supplementary Information), which can be improved in the future by carefully engineering LED structure.

In Ref. [49], Almasi *et al.* also performed chemical mapping on the Mo capped CoFeB/MgO/CoFeB MTJ structure by energy-dispersive X-ray spectroscopy (EDX). Although they have shown that the integrity of the CoFeB layers as well as the MgO barrier was maintained after annealing at 400°C, the atomic layer scale element distribution at the Mo/CoFeB/MgO interface as well as the B information is not possible to be revealed because of the low spatial resolution and energy spectrum range of EDX. Here, by employing advanced STEM combined with high spatial resolved EELS tools, we reveal the information of the structure and local chemical composition of the spin injectors at atomic-layer scale, which is essentially important to understand the measured magnetic and polarization-resolved EL properties and to develop the efficient and optimized electrical spin injection in remanence.

#### 4. Conclusions

In summary, we have developed thermally stable Mo/CoFeB/MgO spin injector for remanent spin injection into GaAs based light emitting diode. A systematic study of magnetic properties, polarization-resolved EL and interfacial structures has been performed and compared with the Ta/CoFeB/MgO spin injector. By using the advanced HR-STEM combined with EELS analyses, we have investigated the interfacial chemical distribution to reveal the mechanism of annealing on the PMA properties of spin-injectors in atomic-scale level. Our findings prove that Mo capped spin-injectors display both high thermal stability of perpendicular magnetic anisotropy and high spin-injection

efficiency even after a 400°C annealing procedure. This type of spin-injector not only has a great potential for future spin-LED and spin laser applications, but also can be widely applied for electrical spin-injection in different kinds of semiconductors and 2D material systems.

#### Conflicts of interest

There are no conflicts to declare.

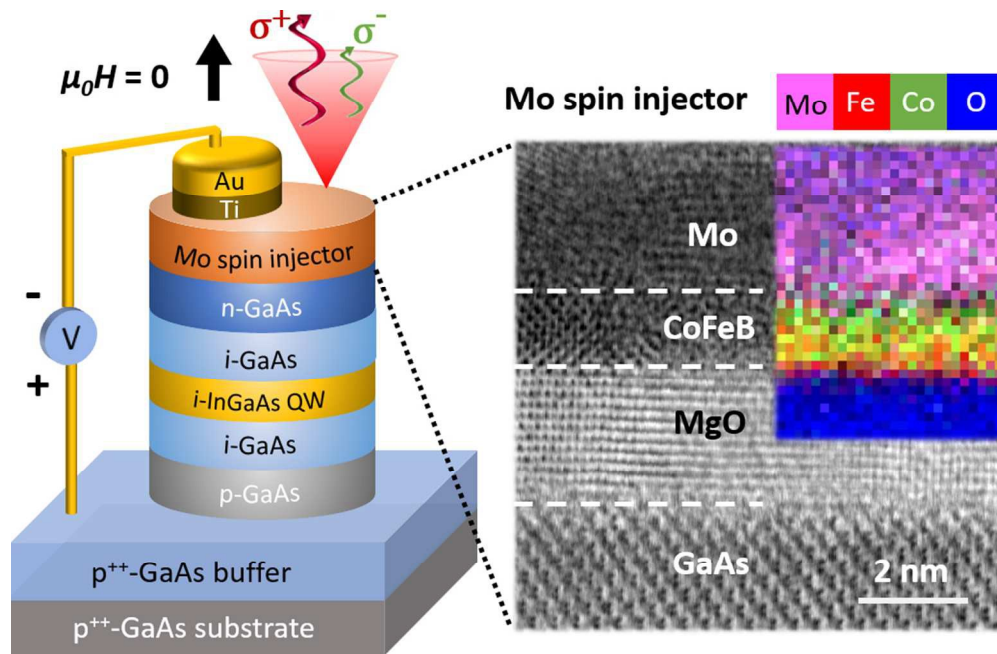
#### Acknowledgements

This work is supported by the joint French National Research Agency (ANR)-National Natural Science Foundation of China (NSFC) SISTER Project (Grant Nos. ANR-11-IS10-0001 and NNSFC 61161130527), ENSEMBLE Project (Grant Nos. ANR-14-0028-01 and NNSFC 61411136001) and by the French PIA project “Lorraine Université d’Excellence”, reference ANR-15-IDEX-04-LUE. X.F.H. also acknowledges support from the NSFC with Grant No. 51620105004 and 11434014. Experiments were performed using equipment from the platform TUBE–Davm funded by FEDER (EU), ANR, the Region Lorraine and Grand Nancy.

#### References

1. M. Holub, P. Bhattacharya, *J. Phys. D: Appl. Phys.* 2007, 40, R179–R203.
2. R. Farshchi, M. Ramsteiner, J. Herfort, A. Tahraoui, H. T. Grahn, *Appl. Phys. Lett.* 2011, 98, 162508.
3. P. Asshoff, A. Merz, H. Kalt, M. Hetterich, *Appl. Phys. Lett.* 2011, 98, 112106.

4. D. Y. Kim, *J. Korean Phys. Soc.* 2006, **49**, S505-S508.
5. R. Fiederling, M. Keim, G. Reuscher, W. Ossau, G. Schmidt, A. Waag, L. W. Molenkamp, *Nature* 1999, **402**, 787-790.
6. Y. Ohno, D. K. Young, B. Beschoten, F. Matsukura, H. Ohno, D. D. Awschalom, *Nature* 1999, **402**, 790-792.
7. H. J. Zhu, M. Ramsteiner, H. Kostial, M. Wassermeier, H.-P. Schönherr, K. H. Ploog, *Phys. Rev. Lett.* 2001, **87**, 016601.
8. A. T. Hanbicki, B. T. Jonker, G. Itkos, G. Kioseoglou, A. Petrou, *Appl. Phys. Lett.* 2002, **80**, 1240-1242.
9. A. T. Hanbicki, O. M. J. van't Erve, R. Magno, G. Kioseoglou, C. H. Li, B. T. Jonker, G. Itkos, R. Mallory, M. Yasar, A. Petrou, *Appl. Phys. Lett.* 2003, **82**, 4092-4094.
10. M. J. van't Erve, G. Kioseoglou, A. T. Hanbicki, C. H. Li, B. T. Jonker, R. Mallory, M. Yasar, A. Petrou, *Appl. Phys. Lett.* 2004, **84**, 4334-4336.
11. C. Adelman, X. Lou, J. Strand, C. J. Palmstrøm, P. A. Crowell, *Phys. Rev. B* 2005, **71**, 121301(R).
12. M. J. van't Erve, G. Kioseoglou, A. T. Hanbicki, C. H. Li, B. T. Jonker, *Appl. Phys. Lett.* 2006, **89**, 072505.
13. N. Nishizawa, H. Muneakata, *J. Appl. Phys.* 2013, **114**, 033507.
14. B. L. Liu, M. Sénès, S. Couderc, J.F. Bobo, X. Marie, T. Amand, C. Fontaine, A. Arnoult, *Physica E*, 2003, **17**, 358-360.
15. L. Lombez, P. Renucci, P. F. Braun, H. Carrère, X. Marie, T. Amand, B. Urbaszek, J. L. Gauffier, P. Gallo, T. Camps, A. Arnoult, C. Fontaine, C. Deranlot, R. Mattana, H. Jaffrès, J.-M. George, P. H. Binh, *Appl. Phys. Lett.* 2007, **90**, 081111.
16. V. F. Motsnyi, J. De Boeck, J. Das, W. Van Roy, G. Borghs, E. Goovaerts, V. I. Safarov, *Appl. Phys. Lett.* 2002, **81**, 265-267.
17. V. F. Motsnyi, P. Van Dorpe, W. Van Roy, E. Goovaerts, V. I. Safarov, G. Borghs, J. De Boeck, *Phys. Rev. B* 2003, **68**, 245319.
18. X. Jiang, R. Wang, R. M. Shelby, R. M. Macfarlane, S. R. Bank, J. S. Harris, S. S. P. Parkin, *Phys. Rev. Lett.* 2005, **94**, 056601.
19. Y. Lu, V.G. Truong, P. Renucci, M. Tran, H. Jaffrès, C. Deranlot, J.-M. George, A. Lemaître, Y. Zheng, D. Demaille, P.-H. Binh, T. Amand, X. Marie, *Appl. Phys. Lett.* 2008, **93**, 152102.
20. V. G. Truong, P. H. Binh, P. Renucci, M. Tran, H. Jaffrès, Y. Lu, C. Deranlot, J.-M. George, A. Lemaître, T. Amand, X. Marie, *Appl. Phys. Lett.* 2009, **94**, 141109.
21. G. Schmidt, D. Ferrand, L. W. Molenkamp, A. T. Filip, B. J. van Wees, *Phys. Rev. B* 2000, **62**, R4790-R4793.
22. E. I. Rashba, *Phys. Rev. B* 2000, **62**, R16267-R16270.
23. A. Fert, H. Jaffrès, *Phys. Rev. B* 2001, **64**, 184420.
24. M. I. Dyakonov, V. L. Perel, In *Optical Orientation*, Vol.8 (Eds: F. Meier, B. P. Zakharchenya), Elsevier Science Publishers B. V.: Amsterdam, 1984, pp 22-24.
25. M. I. Dyakonov, *Spin Physics in Semiconductors*, Springer: Berlin, 2008, pp 12-13.
26. N. C. Gerhardt, S. Hövel, C. Brenner, M. R. Hofmann, F.-Y. Lo, D. Reuter, A. D. Wieck, E. Schuster, W. Keune, K. Westerholt, *Appl. Phys. Lett.* 2005, **87**, 032502.
27. S. Hövel, N. C. Gerhardt, M. R. Hofmann, F.-Y. Lo, A. Ludwig, D. Reuter, A. D. Wieck, E. Schuster, H. Wende, W. Keune, O. Petravic, K. Westerholt, *Appl. Phys. Lett.* 2008, **93**, 021117.
28. L. Grenet, M. Jamet, P. Noé, V. Calvo, J.-M. Hartmann, L. E. Nistor, B. Rodmacq, S. Auffret, P. Warin, Y. Samson, *Appl. Phys. Lett.* 2009, **94**, 032502.
29. J. Zarpellon, H. Jaffrès, J. Frougier, C. Deranlot, J. M. George, D. H. Mosca, A. Lemaître, F. Freimuth, Quang Ha Duong, P. Renucci, X. Marie, *Phys. Rev. B* 2012, **86**, 205314.
30. A. Sinsarp, T. Manago, F. Takano, H. Akinaga, *J. Supercond. Nov. Magn.* 2007, **20**, 405-408.
31. C. Adelman, J. L. Hilton, B. D. Schultz, S. McKernan, C. J. Palmstrøm, X. Lou, H.-S. Chiang, P. A. Crowell, *Appl. Phys. Lett.* 2006, **89**, 112511.
32. S. H. Liang, T. T. Zhang, P. Barate, J. Frougier, M. Vidal, P. Renucci, B. Xu, H. Jaffrès, J.-M. George, X. Devaux, M. Hehn, X. Marie, S. Mangin, H. X. Yang, A. Hallal, M. Chshiev, T. Amand, H. F. Liu, D. P. Liu, X. F. Han, Z. G. Wang, Y. Lu, *Phys. Rev. B* 2014, **90**, 085310.
33. S. Ikeda, K. Miura, H. Yamamoto, K. Mizunuma, H. D. Gan, M. Endo, S. Kanai, J. Hayakawa, F. Matsukura, H. Ohno, *Nat. Mater.* 2010, **9**, 721-724.
34. B. S. Tao, P. Barate, J. Frougier, P. Renucci, B. Xu, A. Djéffal, H. Jaffrès, J.-M. George, X. Marie, S. Petit-Watelot, S. Mangin, X. F. Han, Z. G. Wang, Y. Lu, *Appl. Phys. Lett.* 2016, **108**, 152404.
35. W.G. Wang, S. Hageman, M. Li, S. Huang, X. Kou, X. Fan, J. Q. Xiao, C. L. Chien, *Appl. Phys. Lett.* 2011, **99**, 102502.
36. N. Miyakawa, D. C. Worledge, K. Kita, *IEEE Magn. Lett.* 2013, **4**, 1000104.
37. T. Liu, J. W. Cai, L. Sun, *AIP Adv.* 2012, **2**, 032151.
38. X. Li, G. Yu, H. Wu, P. V. Ong, K. Wong, Q. Hu, F. Ebrahimi, P. Upadhyaya, M. Akyol, N. Kioussis, X. F. Han, P. K. Amiri and K. L. Wang, *Appl. Phys. Lett.* 2015, **107**, 142403.
39. G. -G. An, J. -B. Lee, S. -M. Yang, J.-H. Kim, W. -S. Chung, J. -P. Hong, *Acta Mater.* 2015, **87**, 259-265.
40. T. Liu, Y. Zhang, J. W. Cai, H. Y. Pan, *Sci. Rep.* 2014, **4**, 5895.
41. P. Barate, S. H. Liang, T. T. Zhang, J. Frougier, B. Xu, P. Schieffer, M. Vidal, H. Jaffrès, B. Lépine, S. Tricot, F. Cadiz, T. Garandel, J. M. George, T. Amand, X. Devaux, M. Hehn, S. Mangin, B. Tao, X. F. Han, Z. G. Wang, X. Marie, Y. Lu, P. Renucci, *Phys. Rev. Appl.* 2017, **8**, 054027.
42. P. Barate, S. Liang, T. T. Zhang, J. Frougier, M. Vidal, P. Renucci, X. Devaux, B. Xu, H. Jaffrès, J. M. George, X. Marie, M. Hehn, S. Mangin, Y. Zheng, T. Amand, B. Tao, X. F. Han, Z. Wang, Y. Lu, *Appl. Phys. Lett.* 2014, **105**, 012404.
43. T. Miyajima, T. Ibusuki, S. Umehara, M. Sato, S. Eguchi, M. Tsukada, Y. Kataoka, *Appl. Phys. Lett.* 2009, **94**, 122501.
44. J. Sinha, M. Gruber, M. Kodzuka, T. Ohkubo, S. Mitani, K. Hono, M. Hayashi, *J. Appl. Phys.* 2015, **117**, 043913.
45. Y. Lu, B. Lépine, G. Jézéquel, S. Ababou, M. Alnot, J. Lambert, A. Renard, M. Mullet, C. Deranlot, H. Jaffrès, F. Petroff, J.-M. George, *J. Appl. Phys.* 2010, **108**, 043703.
46. Z. Wang, M. Saito, K. P. McKenna, S. Fukami, H. Sato, S. Ikeda, H. Ohno, Y. Ikuhara, *Nano Lett.* 2016, **16**, 1530-1536.
47. Y. R. Luo, *Comprehensive Handbook of Chemical Bond Energies*, CRC Press, Boca Raton, FL, USA 2007.
48. H. Yang, M. Chshiev, B. Dieny, J. Lee, A. Manchon, K. Shin, *Phys. Rev. B* 2011, **84**, 054401.
49. H. Almasi, D. Reifsnnyder Hickey, T. Newhouse-Illige, M. Xu, M. R. Rosales, S. Nahar, J. T. Held, K. A. Mkhoyan, and W. G. Wang, *Appl. Phys. Lett.* 2015, **106**, 182406.



275x177mm (96 x 96 DPI)